**ORIGINAL PAPER**

# Jouravskite: refined data on the crystal structure, chemical composition and spectroscopic properties

Nikita V. Chukanov[1,2] · Natalia V. Zubkova[2] · Leonid A. Pautov[3] · Jörg Göttlicher[4] · Anatoly V. Kasatkin[3] · Konstantin V. Van[5] · Dmitriy A. Ksenofontov[2] · Igor V. Pekov[2] · Svetlana A. Vozchikova[1] · Dmitry Yu. Pushcharovsky[2]

## Abstract

Refined data on the crystal structure, chemical composition and properties of jouravskite, ideally $Ca_3Mn^{4+}(SO_4)(CO_3)$ $(OH)_6 \cdot 12H_2O$, have been obtained on a sample from N'Chwaning 3 Mine, Kuruman, Kalahari manganese field, Northern Cape Province, South Africa. The chemical composition determined using a combination of different methods (including ICP-OES, gas chromatography of products of ignition and electron microprobe) is (wt%): CaO 25.88, SrO 0.19, BaO 0.23, $B_2O_3$ 0.39, $Fe_2O_3$ 1.01, $MnO_2$ 12.00, $SiO_2$ 0.06, $CO_2$ 6.8, $SO_3$ 12.44, $H_2O$ 41.8, total 100.80, which corresponds to the empirical formula ($Z = 2$): $(Ca_{2.98}Sr_{0.01}Ba_{0.01})_{\Sigma3.00}(Mn^{4+}_{0.89}Fe^{3+}_{0.08}Si_{0.01})_{\Sigma0.98}\{(SO_4)_{1.00}(CO_3)_{1.00}[B(OH)_4]_{0.07}\}_{\Sigma2.07}(OH)_{5.78} \cdot 11.94H_2O$. Tetravalent state of Mn was confirmed by Mn K-edge XANES spectroscopy. The IR spectrum of jouravskite contains characteristic bands of $Mn^{4+}(OH)_6$ octahedra, $CO_3^{2-}$ and $SO_4^{2-}$ anions, and $H_2O$ molecules. The crystal structure was determined using single-crystal X-ray diffraction data and refined to $R = 0.0332$. Jouravskite is isostructural with thaumasite. The parameters of the hexagonal (space group $P6_3$) unit cell are: $a = 11.07129(14)$ Å, $c = 10.62650(14)$ Å, $V = 1128.02(3)$ Å$^3$ and $Z = 3$. Investigation of other samples of ettringite-group minerals from N'Chwaning 3 Mine demonstrates wide variations of the contents of manganese, iron and boron, and possible existence of a $Mn^{4+}$-dominant analogue of sturmanite with the presumed idealized formula $Ca_6Mn^{4+}_2(SO_4)_2[B(OH)_4](OH)_{10}O_2 \cdot nH_2O$.

**Keywords** Jouravskite · Ettringite group · Crystal structure · Chemical composition · IR spectroscopy · XANES spectroscopy · N'Chwaning 3 Mine

✉ Nikita V. Chukanov
chukanov@icp.ac.ru

1. Institute of Problems of Chemical Physics, Russian Academy of Sciences, Chernogolovka, Moscow Region 142432, Russia

2. Faculty of Geology, Moscow State University, Vorobievy Gory, Moscow 119991, Russia

3. Fersman Mineralogical Museum of Russian Academy of Sciences, Leninsky Prospekt 18-2, Moscow 119071, Russia

4. Karlsruhe Institute of Technology, Institute for Photon Science and Synchrotron Radiation (IPS), Hermann-von-Helmholtz-Platz 1, 76344 Eggenstein-Leopoldshafen, Germany

5. Institute of Experimental Mineralogy, Russian Academy of Sciences, Chernogolovka, Moscow Region 142432, Russia

## Introduction

Ettringite-group minerals and related synthetic phases are now in focus of great scientific and technological interest because of their widespread occurrence in both natural environments and cements. Formation of ettringite-related compounds can result in rapid and serious deterioration of cement materials and destruction of concrete constructions, a phenomenon known as "sulfate attack" (Crammond 1985; Day 1992; Batic et al. 2000; Brown and Hooton 2002; Brown et al. 2003; Sims and Huntley 2004). Natural ettringite group members mainly occur in low-temperature hydrothermal, especially epithermal mineral associations that are spatially and genetically related to skarns, calcic xenoliths in effusive rocks, rodingites, different pegmatites, as well as regional-metamorphic rocks (Knill and Young 1960; Gross 1977, 1980; Dunn et al. 1983; Peacor et al. 1983; Grubessi et al. 1986; Hentschel 1993; Malinko et al. 2001; McDonald et al. 2001; Merlino and Orlandi 2001; Kusachi et al.

2008; Chukanov et al. 2012, 2016; Pekov et al. 2012; Nishio-Hamane et al. 2015).

The crystal structures of ettringite-group minerals are based on the infinite $Ca_3[M(OH)_6(H_2O)_m]$ columns formed by $M(OH)_6$ octahedra ($M$ = Si, Ge, $Mn^{4+}$, $Cr^{3+}$, Al, or $Fe^{3+}$) and trimers of edge-sharing Ca-centered polyhedra $Ca(OH)_4(H_2O)_x$ where the value of $x$ and the coordination of Ca depend on the number $n$ of $H_2O$ molecules in the formula (Skoblinskaya et al. 1975). In ettringite-group minerals, the anions $SO_4^{2-}$, $CO_3^{2-}$, $SO_3^{2-}$, $PO_3OH^{2-}$ or $B(OH)_4^-$ are located inside wide channels running parallel to the $c$-axis. Numerous compounds with ettringite-type structure containing different intra-channel anions have been synthesized (Pöllmann et al. 1989; Motzet and Pöllmann 1999).

The ettringite group includes the minerals belonging to different structural types in the frame of the above-described structure archetype. In the structures of the **hexagonal** members of the group with the highest possible space group $P6_3/m$ and small unit cell with $c \approx 11$ Å, namely carraraite $Ca_3Ge(SO_4,CO_3)_2(OH)_6 \cdot 12H_2O$ (Merlino and Orlandi 2001) and kottenheimite $Ca_3Si(SO_4)_2(OH)_6 \cdot 12H_2O$ (Chukanov et al. 2012), tetrahedral ($SO_4$) groups and groups with three-fold coordination of the central atom (subordinate $CO_3$ or $SO_3$) are disordered.

The second type includes **hexagonal** members with the same unit-cell dimensions, but in their structures, intra-channel anions are ordered that causes symmetry lowering to $P6_3$. Ettringite-group minerals belonging to this type are jouravskite $Ca_3Mn^{4+}(SO_4)(CO_3)(OH)_6 \cdot 12H_2O$ (Gaudefroy and Permingeat 1965; Granger and Protas 1969), thaumasite $Ca_3Si(SO_4)(CO_3)(OH)_6 \cdot 12H_2O$ (Effenberger et al. 1983; Martucci and Cruciani 2006), hielscherite $Ca_3Si(SO_4)(SO_3)(OH)_6 \cdot 11H_2O$ (Pekov et al. 2012), imayoshiite $Ca_3Al(CO_3)[B(OH)_4](OH)_6 \cdot 12H_2O$ (Nishio-Hamane et al. 2015) and tatarinovite $Ca_3Al(SO_4)[B(OH)_4](OH)_6 \cdot 12H_2O$ (Chukanov et al. 2016). Minerals belonging to both structure types are characterized by the ratio of the content of $Ca^{2+}$ cations to the sum of intra-channel anions of 3:2. Micheelsenite, ideally $(Ca_2Y)Al(HPO_4)(CO_3)(OH)_6 \cdot 12H_2O$, is the Y-bearing phosphate analogue of thaumasite (McDonald et al. 2001).

The third type includes **trigonal** (space group $P31c$) members of the group, namely ettringite $Ca_6Al_2(SO_4)_3(OH)_{12} \cdot 26H_2O$ (Moore and Taylor 1970), sturmanite $Ca_6Fe^{3+}_2(SO_4)_{2.5}[B(OH)_4](OH)_{12} \cdot 25H_2O$ (Peacor et al. 1983; Pushcharovsky et al. 2004), charlesite $Ca_6(Al,Si)_2(SO_4)_2[B(OH)_4](OH,O)_{12} \cdot 26H_2O$ (Dunn et al. 1983) and its unnamed analogue with $CO_3 > SO_4$ (Kusachi et al. 2008). They have doubled unit-cell parameter $c$ and another stoichiometry: the ratio of the content of $Ca^{2+}$ cations to the sum of intra-channel anions is 2:1.

Current study of jouravskite was undertaken because of a lack of high-quality data on its crystal structure, variations of chemical composition and spectroscopic properties. In particular, data on the structure of this mineral (Granger and Protas 1969) are quite poor (the structure was refined to $R = 16\%$), the valence state of Mn was determined based on indirect data and there are no data published on contents of admixed components (B, Fe, Sr, Ba).

## Samples and experimental methods

### Samples

Three samples from N'Chwaning 3 Mine, Kuruman, Kalahari manganese field, Northern Cape Province, South Africa, were investigated. Preliminary compositional data based on semiquantitative electron microprobe analyses and IR spectra correspond to the approximate stoichiometry $\sim Ca_3(Mn_{0.9}Fe_{0.1})(SO_4)(CO_3)(OH)_x \cdot nH_2O$ (Sample 1), $\sim Ca_3(Mn_{0.6}Fe_{0.4})(SO_4)[B(OH)_4]_{0.6-0.7}(CO_3)_{0.4-0.3}(OH)_x \cdot nH_2O$ (Sample 2) and $\sim Ca_6(Fe_{1.3}Si_{0.4}Mn_{0.2}Al_{0.1})(SO_4)_{2.1}[B(OH)_4]_{0.6-0.7}(CO_3)_{0.1-0.2}(OH)_x \cdot nH_2O$ (Sample 3), which corresponds to jouravskite, a $B(OH)_4$-dominant analogue of jouravskite and sturmanite, respectively.

Samples 1 and 2 contain yellow hexagonal bipyramidal crystals up to 4 and 0.3 mm across, respectively. Both occur in association with bixbyite and calcite. Additionally, in the Sample 1 brucite was identified. The sample 3 used for a comparison forms monomineral aggregate of brownish-yellow hexagonal bipyramidal crystals up to 1.5 cm across. Most of the data have been obtained for Sample 1 (Fig. 1), since Sample 2 is available in amounts insufficient for its detailed study involving precise determination of light elements (H, C and B).



**Fig. 1** Crystals of jouravskite (yellow, sample 1) in association with bixbyite (black crystals), calcite (white) and brucite (brownish). Field width 2 cm. Photo: A. D. Kasatkina

## Mn *K*-edge XANES spectroscopy

The Mn *K*-edge XANES spectroscopy was applied for the determination of Mn valence state in jouravskite. The spectra were recorded at the X-ray beamline of the Synchrotron Radiation Laboratory for Environmental Studies (SUL-X) of the synchrotron radiation source ANKA (Karlsruhe Institute of Technology, KIT).

Initially, several grains 0.2–0.4 mm in size were crushed to enable the recording of spectra averaged on crystallographic orientations. The ground material was fixed on Kapton tape. In another experiment, a single crystal was used with one of its faces parallel to the tape surface. The tape was arranged at 45° to the incoming beam and the fluorescence detector, allowing simultaneous measurements in transmission and fluorescence mode. The storage ring operated at electron energy of 2.5 GeV. A 27 pole wiggler was used as the radiation source. A Si(111) crystal pair has been used as double-crystal monochromator with fixed beam height. Sample spectra were measured in transmission only or in transmission and fluorescence using ionization chambers in front and behind the sample, and a seven-element Si(Li) solid-state detector (SGX Sensortech, former Gresham) for recording the Mn $K_\alpha$ fluorescence emission signal. Due to the small sample amounts, the synchrotron beam was focused with Kirk-Patrick–Baez mirrors to a beam size at sample position of about 100 μm horizontally and about 70 μm vertically. The first ionization chamber was used both in transmission and fluorescence modes for normalization of the absorption and fluorescence intensities. Energy has been calibrated to 6539 eV (the first inflection point of Fe *K* XANES spectra of a Mn foil measured simultaneously to samples with the second and third ionization chamber).

Transmission data have been preferred for evaluation because some of the fluorescence data were slightly affected by self-absorption. XANES spectra were recorded in energy steps of 5 eV from −150 to −50 eV and of 2 eV from −50 to −20 eV prior to the edge, of 0.3 eV from −20 to +20 eV across the edge, and with a *k* step of 0.05 from *k* 2.29 to at least *k* 8.3 (+20 to about +260 eV) above the edge. To increase the signal to noise ratio, scans have been repeated as necessary. Spectra were pre- and post-edge background corrected and normalized using the ATHENA program of the Ifeffit software package (Ravel and Newville 2005).

Several measurements were made for the crushed material at different sample positions and one measurement for the single crystal (Fig. 2). For the comparison of the sample edge position with the edge positons of Mn *K* XANES spectra of reference substances, the spectra of the crushed sample were used because they average spectral shapes of different crystal orientations although the spectrum of the single crystal did not show any difference to the spectrum of the crushed material. Reference spectra for compounds
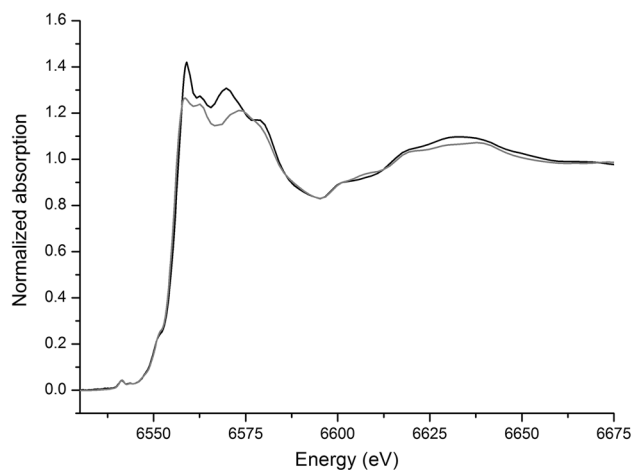


**Fig. 2** Comparison of Mn *K* XANES spectra of crushed crystals (black) and single crystal (grey)

of Mn in different valence states were used for comparison with the sample spectrum.

## Infrared spectroscopy

To obtain IR absorption spectra, hand-picked grains were ground in an agate mortar, mixed with anhydrous KBr, pelletized, and analyzed using an ALPHA FTIR spectrometer (Bruker Optics) in the range of wavenumbers from 360 to 3800 cm$^{-1}$, with a spectral resolution of 4 cm$^{-1}$. The IR spectrum of a pure KBr disk was used as a reference. The assignment of absorption bands was made according to Pöllmann et al. (1989), Chukanov et al. (2012, 2016), and Chukanov and Chervonnyi (2016).

## Chemical composition

Initial semiquantitative compositional data on a jouravskite sample from N'Chwaning 3 Mine were obtained by means of a Tescan VEGA-II XMU INCA Energy 450 (EDS mode, 20 kV, 190 pA, 180 nm beam diameter). It was found that only six elements (Ca, Ba, Mn, Fe, Si and S) are present in the mineral in quantities exceeding the detection limit. The standards used were $FeS_2$ for S, $BaF_2$ for Ba, wollastonite for Ca, quartz for Si, and pure Mn and Fe for corresponding elements. The limits of the contents of corresponding components are (wt%): BaO 0–0.40, CaO 26.83–28.37, $SiO_2$ 0–0.15, $MnO_2$ 11.20–13.21, $Fe_2O_3$ 1.21–1.44, $SiO_2$ 0–0.17, $SO_3$ 12.59–13.48. Jouravskite is unstable under the electron beam, which leads to a large error in the analysis and an overestimation of the analytical total due to partial dehydration of the mineral.

The precise chemical composition was determined using a VARIAN 725 ICP-OES instrument with axial plasma

viewing, at a power of 1200 W. For this, the mineral grains with a total weight of 4.43 mg were dissolved in a closed polypropylene bottle at room temperature in 4 ml of hydrochloric acid 1:1 (Ultrapur Merck). The solution was brought to 100.0 ml with 18.2-m$\Omega$-grade deionized water. Calibration solutions in 2% hydrochloric acid were prepared from the multicomponent standard solutions (Merck).

$H_2O$, $CO_2$ and N were analysed by gas chromatography of products of ignition in oxygen at 1200 °C with a Vario Micro Cube analyser (Elementar GmbH, Germany). The content of nitrogen in the studied sample is below detection limit of the method.

## Single-crystal X-ray diffraction

Single-crystal X-ray studies of jouravskite (Sample 1) were carried out using an Xcalibur S diffractometer equipped with a CCD detector at room temperature. A full sphere of three-dimensional data was collected. Data reduction was performed using CrysAlisPro Version 1.171.37.34 (Agilent Technologies 2014). The data were corrected for Lorentz and polarization effects. The crystal structure was solved by direct methods and refined with the use of SHELX-97 software package (Sheldrick 2008) with neutral atom scattering factors to $R = 0.0332$ for 2245 unique reflections with $I > 2\sigma(I)$. Hydrogen atoms of OH groups and water molecules were found from the difference Fourier synthesis, O–H distances were restrained to 0.85(1) Å (H···H distances for $H_2O$ molecules were restrained to 1.37(1) Å) and their equivalent atomic displacement parameter ($U_{eq}$) was set to 1.2 Ueq of the corresponding donor O atom. $B(OH)_4$ tetrahedra were not localized due to their very minor amount.

## Results

### Mn *K*-edge XANES spectroscopy

There is a correlation of the centroid position of the pre-edge peak(s) with Mn valence (Chalmin et al. 2009). A comparison of the Mn *K*-edge X-ray absorption fine structure (XAFS) spectra of the sample spectrum of the crushed crystals with Mn(IV), Mn(III) and Mn(II) reference spectra (Fig. 3) shows that the edge position of the jouravskite spectrum is close to that of pyrolusite $MnO_2$ used as a Mn(IV) reference, but differs in shape from the latter. Obviously, these differences are caused by different local situations involving $Mn^{4+}$: $MnO_6$ octahedra in pyrolusite and $Mn(OH)_6$ octahedra in jouravskite.

When using the edge shift as a measure for Mn valence, constructive and destructive interferences between atomic absorption with multiple-scattering features from distant neighbors can be a source of error (Farges 2005; Chalmin
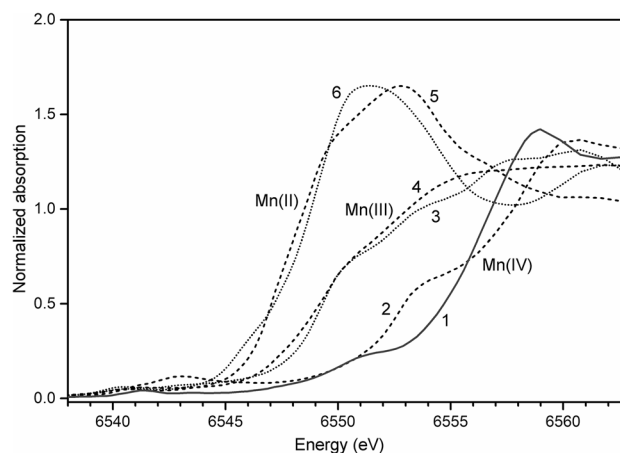


**Fig. 3** Mn *K* XANES spectra of studied jouravskite (1), pyrolusite $MnO_2$ (2), manganite MnOOH (3), purpurite $(Mn^{3+},Fe^{3+})PO_4$ (4), synthetic $Mn^{2+}SO_4 \cdot nH_2O$ (5) and rhodochrosite $Mn^{2+}CO_3$ (6)

et al. 2009). On the other hand, if one compares the jouravskite spectrum with some more references from the literature (Manceau et al. 2012), there are no indications for significant contribution of Mn(II) and/or Mn(III) to the jouravskite spectrum. The spectra of Mn(III) references are close to each other independent of their chemistry and structure, whereas Mn *K* XANES jouravskite and the three Mn(IV) references from Manceau et al. (2012), i.e., $CaMn_3O_8$, ramsdellite ($MnO_2$) and pyrolusite ($MnO_2$) show significant higher edge positions than the Mn(III) reference spectra.

## Infrared absorption spectroscopy

IR spectra of ettringite-group minerals from N'Chwaning 3 Mine are presented in Fig. 4, and assignment of absorption bands is given in Table 1.

A characteristic feature of the jouravskite spectrum is the presence of bands at 3085 and 3245 cm$^{-1}$ corresponding to strong hydrogen bonds. The assignment of weak bands observed in IR spectra of all ettringite-group minerals in the range from 2100 to 2500 cm$^{-1}$ is ambiguous. It is doubtful that these bands belong to overtones or combination modes, given their large widths which are characteristic of the bands of acid OH groups.

Most probably, transitions of this kind are due to the dynamic equilibrium $SO_4^{2-} + H_2O \leftrightarrow HSO_4^- + OH^-$. Proton transition of such kind is usual in crystals of hydrous nominally neutral oxysalts, and the dynamic equilibrium is usually significantly shifted to the left (Chukanov and Chervonnyi 2016).

In the series Sample 1 $\rightarrow$ Sample 2 $\rightarrow$ Sample 3, a number of regular changes in the parameters of the IR spectra are observed:
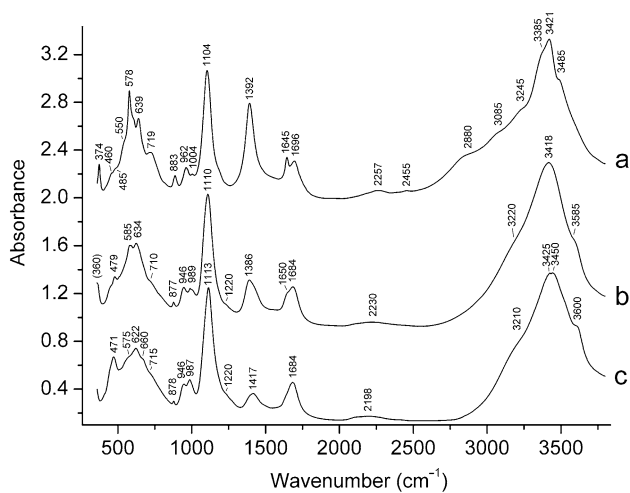
**Fig. 4** Powder IR absorption spectra of Sample 1 (**a**), Sample 2 (**b**) and Sample 3 (**c**)

- The doublet of H–O–H bending vibrations is converted to a singlet, whereas bands of strong hydrogen bonds in the range from 2800 to 3100 $cm^{-1}$ disappear. Consequently, the bands at 1645, 3085 and 3245 $cm^{-1}$ can be assigned to $H_2O$ molecules forming strong hydrogen bonds (see "Discussion" section below).
- The bands of $CO_3^{2-}$ anions become weaker, whereas the intensities of the bands of $B(OH)_4^-$ anions increase.
- The band of $Fe^{3+}$–O-stretching vibrations (at 471–479 $cm^{-1}$) appears and intensifies, while the band of the $Mn^{4+}$–O-stretching vibrations (at 578–585 $cm^{-1}$) becomes weaker and transforms into the shoulder at 575 $cm^{-1}$.

All these regularities are in agreement with the chemical composition of the samples studied. Based on these data, Sample 2 can be considered as a potentially new mineral species, a $B(OH)_4^-$-dominant analogue of jouravskite or a $Mn^{4+}$-dominant analogue of sturmanite, with the idealized formula $Ca_6Mn^{4+}_2(SO_4)_2[B(OH)_4](OH)_{10}O_2 \cdot nH_2O$. Unfortunately, the small amount of the substance did not allow performing a detailed study of this mineral.

The assignment of the band at 962 $cm^{-1}$ in the IR spectrum of Sample 1 is mostly difficult. Based on data on the chemical composition, it can be assumed that this band refers to stretching vibrations of admixed $SO_3^{2-}$ anions. For example, in the IR spectrum of hannebachite $CaSO_3 \cdot 0.5H_2O$, these vibrations give rise to the strong doublet $944 + 984$ $cm^{-1}$. However, in the IR spectrum of the $SO_3$-dominant ettringite-group mineral hielscherite, the strongest band of $S^{4+}$–O-stretching vibrations is observed at 937 $cm^{-1}$, whereas the band at 967 $cm^{-1}$ has a low intensity (Chukanov 2014). Another possibility, which seems more convincing to us, is that the band at 962 $cm^{-1}$ should be assigned to $Mn^{4+}$–O–H bending vibrations.

## Chemical composition

Analytical data for jouravskite (Sample 1) are given in Table 2. Contents of other elements are below detection limits.

The empirical formula calculated on the basis of 25 O atoms is $(Ca_{2.98}Sr_{0.01}Ba_{0.01})_{\Sigma 3.00}(Mn^{4+}_{0.89}Fe^{3+}_{0.08}Si_{0.01})_{\Sigma 0.98}\{(SO_4)_{1.00}(CO_3)_{1.00}[B(OH)_4]_{0.07}\}_{\Sigma 2.07}(OH)_{5.78} \cdot 11.94H_2O$. As it was noted above, based on IR spectroscopic data, a minor

**Table 1** Assignment of absorption bands ($cm^{-1}$) in the IR spectra of ettringite group from N'Chwaning 3 Mine

| Sample 1 | Sample 2 | Sample 3 | Kind of vibrations |
|---|---|---|---|
| 3485sh, 3421s, 3385sh, 3245sh, 3085sh, 2880sh | 3583sh, 3418s, 3220sh | 3600sh, 3450s, 3425s, 3210sh | O–H stretching ($H_2O$ molecules and $OH^-$ anions) |
| 2455w, 2257w | 2230w | 2198w | O–H stretching (acid OH groups) |
| 1696, 1645 | 1684, 1650sh | 1684 | H–O–H bending |
| 1392s | 1386 | 1417 | Stretching vibrations of $CO_3^{2-}$ anions |
|  | 1220sh | 1220sh | B–O-stretching [trace amounts of $B(OH)_3$ groups?] |
| 1104s | 1110s | 1113s | Asymmetric stretching ($SO_4^{2-}$ anions) |
| 1004w | ~1000sh |  | Symmetric stretching ($SO_4^{2-}$ anions) |
| 962 |  |  | Presumably, stretching vibrations of admixed $SO_3^{2-}$ anions |
|  | 989, 946 | 987, 946 | B–O-stretching [$B(OH)_4^-$ anions] |
| 883 | 877w | 878w | Out-of-plane bending ($CO_3^{2-}$ anions) |
| 719 | 710sh | 715sh | In-plane bending ($CO_3^{2-}$ anions) |
| 639s | 634s | 660sh, 622s | Bending ($SO_4^{2-}$ anions) |
| 578s, 550sh | 585 | 575sh | $Mn^{4+}$–O-stretching |
| 485sh, 460sh | 479 | 471s | $Fe^{3+}$–O-stretching |
| 374 | (360) |  | Lattice mode involving libration and Ca–O-stretching vibrations |

*s* strong band, *w* weak band, *sh* shoulder

**Table 2** Chemical composition of jouravskite

| Component | Content (wt%) | |
| --- | --- | --- |
| | Sample 1 (this work) | Gaudefroy and Permingeat (1965)[a] |
| CaO | 25.88 | 25.67 |
| SrO | 0.19 | No data |
| BaO | 0.23 | No data |
| $B_2O_3$ | 0.39 | No data |
| $Fe_2O_3$ | 1.01 | No data |
| $MnO_2$[b] | 12.00 | 14.78 |
| $SiO_2$[c] | 0.06 | 0 |
| $CO_2$ | 6.8 | 7.45 |
| $SO_3$ | 12.44 | 10.20 |
| $H_2O$ | 41.8 | 41.90 |
| Total | 100.80 | 100.00 |

[a]Holotype sample with manganite impurity from Tachgagalt No 2 vein (Anti-Atlas, Morocco)

[b]According to XANES data, manganese is tetravalent

[c]From electron microprobe data

substitution of $SO_4^{2-}$ for $SO_3^{2-}$ cannot be excluded, but is hardly probably taking into account comparison with the $SO_3^{2-}$-dominant ettringite-group mineral hielscherite. A slightly overestimated sum of intra-channel anions is most likely due to the overestimation of $CO_2$ content due to the contribution of atmospheric carbon dioxide adsorbed on the walls of the measuring cell.

## X-ray diffraction data and crystal structure

The unit-cell parameters and the experimental details are presented in Table 3, atom coordinates and equivalent displacement parameters in Table 4, selected interatomic distances in Table 5 and hydrogen bonding geometry in Table 6. Bond-valence calculations (Table 7) were performed using the parameters from Gagné and Hawthorne (2015) and from Ferraris and Ivaldi (1988) for H-bonding.

Like in other members of ettringite group the crystal structure of jouravskite (Fig. 5) is characterized by the presence of columns running along [001] and formed by alternating $Mn(OH)_6$ octahedra and triplets of Ca-centered eightfold polyhedra $Ca(OH)_4(H_2O)_4$ (Fig. 6). In jouravskite, these columns have the composition $[Ca_3Mn^{4+}(OH)_6(H_2O)_{12}]^{4+}$. Alternating along [001], ordered $SO_4$ tetrahedra and $CO_3$ triangles are located among the columns and all O atoms of these groups are involved in the complicate system of hydrogen bonds (Table 6).

**Table 3** Crystal data, data collection information and structure refinement details for jouravskite (Sample 1)

| Crystal data | |
| --- | --- |
| Formula | $Ca_3Mn^{4+}(SO_4)(CO_3)(OH)_6·12H_2O$ |
| Formula weight (g) | 649.49 |
| Temperature (K) | 293(2) |
| Cell setting | Hexagonal |
| Space group | $P6_3$ (No. 173) |
| Lattice parameters | |
| $a$ (Å) | 11.07129(14) |
| $c$ (Å) | 10.62650(14) |
| $V$ (Å³) | 1128.02(3) |
| $Z$ | 2 |
| Crystal size (mm) | $0.08 \times 0.20 \times 0.27$ |
| Data collection | |
| Diffractometer | Xcalibur S CCD |
| Radiation; $\lambda$ (Å) | Mo$K_\alpha$; 0.71073 |
| Absorption coefficient, $\mu$ (mm⁻¹) | 1.465 |
| Absorption correction | Multi-scan |
| | Empirical absorption correction using spherical harmonics, implemented in SCALE3 ABSPACK scaling algorithm |
| $F$ (000) | 674 |
| Data range $\theta$ (°); $h, k, l$ | 2.86–30.50; $-15 < h < 15$, $-15 < k < 15$ $-15 < l < 15$ |
| No. of measured reflections | 23,169 |
| Unique reflections/observed reflections | 2301/2245 |
| $R_{int}$ (%) | 4.55 |
| $R_\sigma$ (%) | 2.16 |
| Criterion for observed reflections | $I > 2\sigma(I)$ |
| Refinement | |
| Refinement on | Full-matrix least-squares on $F^2$ |
| Weight scheme | $w = 1/[\sigma^2(F_o^2) + (0.0400P)^2 + 1.3603P]$; $P = ([$max of (0 or $F_o^2)] + 2F_c^2)/3$ |
| No. of refinement parameters | 124 |
| Final $R$ indices $[I > 2\sigma(I)]$ | $R1 = 0.0332$, w$R2 = 0.0831$ |
| $R$ indices (all data) | $R1 = 0.0344$, w$R2 = 0.0839$ |
| GOF (goodness of fit) | 1.058 |
| Min./max. residual $e$ density, ($e$ Å⁻³) | –0.47/1.21 |
| Flack | 0.04(4) |

## Discussion

In general, the crystal structure refinement for Sample 1 confirms the structure model of jouravskite obtained by Granger and Protas (1969) which was obtained as a result of the

**Table 4** Atom coordinates (*xyz*), site multiplicities (*Q*) and equivalent atomic displacement parameters ($U_{eq}$, Å$^2$) in the structure of jouravskite (Sample 1)

| Site | $x$ | $y$ | $z$ | $Q$ | $U_{eq/iso}$[a] |
|------|-----|-----|-----|-----|---------|
| Mn | 0.0 | 0.0 | 0.00721(8) | 2 | 0.00942(11) |
| Ca | 0.19695(4) | 0.99005(4) | 0.25711(8) | 6 | 0.01318(10) |
| S | 1/3 | 2/3 | 0.99374(12) | 2 | 0.0164(2) |
| C | 1/3 | 2/3 | 0.4746(5) | 2 | 0.0184(10) |
| Ow1 | 0.3970(2) | 0.2330(2) | 0.2571(4) | 6 | 0.0342(4) |
| H1a | 0.382(3) | 0.299(2) | 0.239(5) | 6 | 0.041[a] |
| H1b | 0.4789(19) | 0.270(3) | 0.288(4) | 6 | 0.041[a] |
| Ow2 | 0.2603(2) | 0.40609(18) | 0.2577(3) | 6 | 0.0287(4) |
| H2a | 0.275(4) | 0.457(4) | 0.194(2) | 6 | 0.034[a] |
| H2b | 0.307(4) | 0.460(4) | 0.318(2) | 6 | 0.034[a] |
| Ow3 | 0.0023(2) | 0.3396(3) | 0.0774(3) | 6 | 0.0245(6) |
| H3a | −0.0792(15) | 0.326(3) | 0.063(4) | 6 | 0.029[a] |
| H3b | 0.056(3) | 0.4270(12) | 0.081(4) | 6 | 0.029[a] |
| Ow4 | 0.0203(3) | 0.3479(3) | 0.4335(3) | 6 | 0.0300(7) |
| H4a | −0.054(2) | 0.351(4) | 0.448(4) | 6 | 0.036[a] |
| H4b | 0.089(2) | 0.428(2) | 0.455(4) | 6 | 0.036[a] |
| OH1 | 0.1378(2) | 0.1331(2) | 0.1177(2) | 6 | 0.0138(4) |
| H1 | 0.215(2) | 0.193(3) | 0.088(4) | 6 | 0.017[a] |
| OH2 | 0.1380(2) | 0.1325(2) | 0.3963(2) | 6 | 0.0142(4) |
| H2 | 0.202(3) | 0.190(3) | 0.444(3) | 6 | 0.017[a] |
| O1 | 0.2015(3) | 0.6221(4) | 0.4669(3) | 6 | 0.0417(8) |
| O2 | 0.1917(3) | 0.6231(3) | 0.0407(3) | 6 | 0.0285(5) |
| O3 | 1/3 | 2/3 | 0.8552(4) | 2 | 0.0277(8) |

All hydrogen atoms were found in the difference Fourier synthesis, O–H distances were restrained to 0.85(1) Å [H···H distances for H$_2$O molecules were restrained to 1.37(1) Å] and their temperature factor was set to $1.2U_{eq}$(O)

[a] $U_{iso}$

**Table 5** Selected interatomic distances (Å) in the structure of jouravskite (Sample 1)

| | |
|---|---|
| Mn–OH1 | 1.905(2)×3 |
| –OH2 | 1.907(2)×3 |
| Ca–Ow4 | 2.405(3) |
| –Ow3 | 2.437(3) |
| –OH1 | 2.459(2) |
| –OH2 | 2.475(2) |
| –OH1 | 2.484(2) |
| –Ow1 | 2.486(2) |
| –Ow2 | 2.5365(18) |
| S–O3 | 1.472(4) |
| –O2 | 1.478(3)×3 |
| C–O1 | 1.288(3)×3 |

**Table 6** Hydrogen-bond geometry (Å,°) in the structure of jouravskite (Sample 1)

| *D*–H···*A* | *D*–H | H···*A* | *D*···*A* | ∠(*D*–H···*A*) |
|-------------|-------|---------|-----------|----------------|
| Ow1–H1a···Ow2 | 0.846(10) | 2.21(2) | 2.977(3) | 151(4) |
| Ow1–H1b···O3 | 0.851(10) | 1.968(10) | 2.814(3) | 173(3) |
| Ow2–H2a···O2 | 0.845(10) | 2.01(2) | 2.810(4) | 157(4) |
| Ow2–H2b···O1 | 0.855(10) | 1.952(13) | 2.796(5) | 169(4) |
| Ow3–H3a···O1 | 0.850(10) | 2.00(2) | 2.758(4) | 148(3) |
| Ow3–H3b···O2 | 0.847(10) | 1.972(16) | 2.797(4) | 164(4) |
| Ow4–H4a···O2 | 0.848(10) | 1.96(2) | 2.768(4) | 159(4) |
| Ow4–H4b···O1 | 0.858(10) | 1.878(19) | 2.698(5) | 160(4) |
| OH1–H1···Ow4 | 0.840(10) | 2.21(2) | 2.978(4) | 152(4) |
| OH2–H2···Ow3 | 0.844(10) | 2.123(12) | 2.960(4) | 171(4) |

In our case, SO$_4$ tetrahedron is much more regular [with three S–O distances of 1.472(4) Å and the fourth one equal to 1.478(3) Å, and with O–S–O angles of 109.73(12) and 109.21(12)°], whereas in the initial structure model SO$_4$ tetrahedron was distorted, with three S–O bonds having the distances of 1.41(3) Å, the fourth one equal to 1.55(9) Å and O–S–O angles equal to 107.7 and 111.1°. The CO$_3$ triangle in Sample 1 is characterized by significantly smaller C–O distances of 1.288(3) Å compared with the value of 1.36(5) Å obtained by Granger and Protas (1969). This results in better values of bond-valence sums of 3.96 v.u. for C in Sample 1. Bond-valence calculations also confirm tetravalent state of Mn in jouravskite (Table 7).

As noted above, the shoulders at 2880 and 3085 cm$^{-1}$ in the IR spectrum of jouravskite may correspond to strong hydrogen bonds Mn$^{4+}$OH···OH$_2$. Structural data confirm this assumption: corresponding *D*···*A* distances are rather short and are equal to 2.978 and 2.960 Å (Table 6). A shoulder below 3100 cm$^{-1}$ is observed also in the IR spectrum of thaumasite from the Uraveli river, near Akhaltsikhe, Georgia (Chukanov 2014) which corresponds to the *D*···*A* distances of 2.936 and 2.939 Å for the hydrogen bonds Si$^{4+}$OH···OH$_2$ in thaumasite (Effenberger et al. 1983). However, no shoulders of O–H-stretching vibrations below 3100 cm$^{-1}$ are observed ithe IR spectrum of sturmanite (Fig. 4) for which the *D*···*A* distances of the hydrogen bonds Fe$^{3+}$OH···OH$_2$ are significantly longer and are equal to 3.07, 3.18, 3.22 and 3.37 Å (Pushcharovsky et al. 2004).

It is to be noted that yellow colour is unusual for a mineral containing manganese in the tetravalent state. Most Mn$^{4+}$ minerals are opaque dark brown or black because of charge transfer between Mn$^{4+}$ and other cations. The only other example is the fleischerite-group mineral despujolsite, Ca$_3$Mn$^{4+}$(SO$_4$)$_2$(OH)$_6$·3H$_2$O. Both of these minerals have isolated Mn$^{4+}$(OH)$_6$ octahedra that do not have close contacts with cations of variable valence, and this is an obvious cause of the light colour.

crystal structure refinement to $R = 16\%$ based on 736 reflections. The most significant differences are connected with the arrangement of atoms in anionic groups SO$_4$ and CO$_3$.

**Table 7** Bond-valence calculations for jouravskite (Sample 1)

| Site | Mn | Ca | S | C | Σ | H–bonding | Σ |
|---|---|---|---|---|---|---|---|
| Ow1 = H$_2$O | | 0.24 | | | 0.24 | −0.13(Ow2); −0.18(O3) | −0.07 |
| Ow2 = H$_2$O | | 0.21 | | | 0.21 | +0.13(Ow2); −0.18(O2); −0.19(O1) | −0.03 |
| Ow3 = H$_2$O | | 0.27 | | | 0.27 | −0.20(O1); −0.18(O2); +0.14(OH2) | 0.03 |
| Ow4 = H$_2$O | | 0.30 | | | 0.30 | −0.20(O2); −0.23(O1); +0.13(OH1) | 0.00 |
| OH1 = OH | 0.66$^{×3↓}$ | 0.26 0.24 | | | 1.16 | −0.13(Ow4) | 1.03 |
| OH2 = OH | 0.66$^{×3↓}$ | 0.26 0.25 | | | 1.17 | −0.14(Ow3) | 1.03 |
| O1 | | | | 1.32$^{×3↓}$ | 1.32 | +0.19(Ow2); +0.20(Ow3); +0.23(Ow4) | 1.81 |
| O2 | | | 1.48$^{×3↓}$ | | 1.48 | +0.18(Ow2); +0.18(Ow3); +0.20(Ow4) | 2.04 |
| O3 | | | 1.50 | | 1.50 | +0.18(Ow1)$^{×3→}$ | 2.04 |
| Σ | 3.96 | 2.03 | 5.94 | 3.96 | | | |
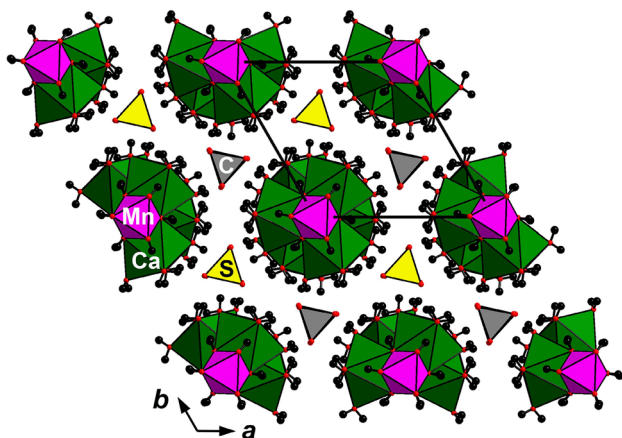


**Fig. 5** The crystal structure of jouravskite in *ab* projection. Oxygen and hydrogen atoms are shown with red and black circles, respectively. The unit cell is outlined
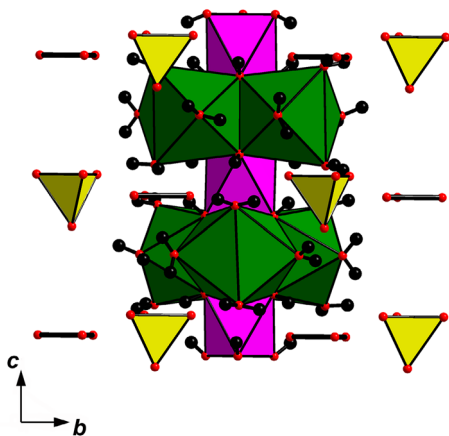


**Fig. 6** The column formed by alternating Mn(OH)$_6$ octahedra and triplets of Ca-centered eightfold polyhedra Ca(OH)$_4$(H$_2$O)$_4$ in the environment of ordered SO$_4$ tetrahedra and CO$_3$ triangles. For legend see Fig. 5

## References

Batic OR, Milanesi CA, Maiza PJ, Marfil SA (2000) Secondary ettringite formation in concrete subjected to different curing conditions. Cement Concr Res 30:1407–1412

Brown PW, Hooton RD (2002) Ettringite and thaumasite formation in laboratory concretes prepared using sulfate-resisting cements. Cement Concr Compos 24:361–370

Brown PW, Hooton RD, Clark BA (2003) The co-existence of thaumasite and ettringite in concrete exposed to magnesium sulfate at room temperature and the influence of blast-furnace slag substitution on sulfate resistance. Cement Concr Compos 25:939–945

Chalmin E, Farges F, Brown GE Jr (2009) A pre-edge analysis of Mn K-edge XANES spectra to help determine the speciation of manganese in minerals and glasses. Contrib Mineral Petrol 157:111–126

Chukanov NV (2014) Infrared spectra of mineral species: extended library. Springer, Dordrecht

Chukanov NV, Chervonnyi AD (2016) Infrared spectroscopy of minerals and related compounds. Springer, Cham

Chukanov NV, Britvin SN, Van KV, Möckel S, Zadov AE (2012) Kottenheimite, Ca$_3$Si(SO$_4$)$_2$(OH)$_6$·12H$_2$O, a new ettringite-group mineral from the Eifel area, Germany. Can Mineral 50:55–63

Chukanov NV, Kasatkin AV, Zubkova NV, Britvin SN, Pautov LA, Pekov IV, Varlamov DA, Bychkova YaV, Loskutov AB, Novgorodova EA (2016) Tatarinovite Ca$_3$Al(SO$_4$)[B(OH)$_4$](OH)$_6$·12H$_2$O, a new ettringite-group mineral from Bazhenovskoe deposit, central Urals, Russia, and its crystal structure. Geol Ore Depos 58(8):653–665

Crammond NJ (1985) Thaumasite in failed cement mortars and renders from exposed brickwork. Cement Concr Res 15:1039–1050

Day RL (1992) The effect of secondary ettringite formation on the durability of concrete: a literature analysis. Portland Cement Association, Skokie

Dunn PJ, Peacor DR, Leavens PB, Baum JL (1983) Charlesite, a new mineral of the ettringite group, from Franklin, New Jersey. Am Mineral 68:1033–1037

Effenberger H, Kirfel A, Will G, Zobetz E (1983) A further refinement of the crystal structure of thaumasite, Ca$_3$Si(OH)$_6$(SO$_4$)(CO$_3$)·12H$_2$O. N Jb Miner Mh 60–68

Farges F (2005) Ab initio and experimental pre-edge investigations of the Mn K-edge XANES in oxide-type materials. Phys Rev B 71(155109):1–14

Ferraris G, Ivaldi G (1988) Bond valence vs bond length in O···O hydrogen bonds. Acta Cryst B 44:341–344

Gagné OC, Hawthorne FC (2015) Comprehensive derivation of bond-valence parameters for ion pairs involving oxygen. Acta Cryst B71:562–578

Gaudefroy C, Permingeat F (1965) La jouravskite, une nouvelle espèce minérale. Bull Soc fr Minéral 88:254–262 **(French)**

Granger MM, Protas J (1969) Détermination et étude de la structure cristalline de la jouravskite $Ca_3Mn^{IV}(SO_4)(CO_3)(OH)_6 \cdot 12H_2O$. Acta Cryst 25:1943–1951

Gross S (1977) The mineralogy of the Hatrurim Formation, Israel. Geol Sur Israel Bull 70:25–26

Gross S (1980) Bentorite. A new mineral from the Hatrurim Area, west of the Dead Sea, Israel. Israel J Earth Sci 29:81–84

Grubessi O, Mottana A, Paris E (1986) Thaumasite from the Tschwinning [N'Chwaning] mine, South Africa. Tschermaks Mineral Petrog Mitt 35:149–156

Hentschel G (1993) Die Lavaströme der Graulai: eine neue Fundstelle in der Westeifel. Lapis 18(9):11–23

Knill DC, Young BR (1960) Thaumasite from Co. Down, Northern Ireland. Mineral Mag 32:416–418

Kusachi I, Shiraishi N, Shimada K, Ohnishi M, Kobayashi S (2008) $CO_3$-rich charlesite from the Fuka mine, Okayama Prefecture, Japan. J Mineral Petrol Sci 103:47–51

Malinko SV, Chukanov NV, Dubinchuk VT, Zadov AE, Koporulina EV (2001) Buryatite, $Ca_3(Si,Fe^{3+},Al)[SO_4](OH)_5O \cdot 12H_2O$, a new mineral. Zapiski Rossiiskogo Mineralogicheskogo Obshchestva (Proc Rus Mineral Soc) 130(2):72–78 (Russian)

Manceau A, Marcus MA, Grangeon S (2012) Determination of Mn valence states in mixed-valent manganates by XANES spectroscopy. Am Mineral 97:816–827

Martucci A, Cruciani G (2006) In situ time resolved synchrotron powder diffraction study of thaumasite. Phys Chem Miner 33:723–731

McDonald AM, Petersen OV, Gault RA, Johnsen O, Niedermayr G, Brandstätter F, Giester G (2001) Micheelsenite, $(Ca,Y)_3Al(PO_3OH,CO_3)(CO_3)(OH)_6 \cdot 12H_2O$, a new mineral from Mont Saint-Hilaire, Quebec, Canada and the Nanna pegmatite, Narsaarsuup Qaava, South Greenland. N Jb Min Mh 337–351

Merlino S, Orlandi P (2001) Carraraite and zaccagnaite, two new minerals from the Carrara marble quarries: their chemical compositions, physical properties, and structural features. Am Mineral 86:1293–1301

Moore AE, Taylor HFW (1970) Crystal structure of ettringite. Acta Cryst B26:386–393

Motzet H, Pöllmann H (1999) Synthesis and characterization of sulfite-containing AFm phases in the system $CaO–Al_2O_3–SO_2–H_2O$. Cement Concr Res 29:1005–1011

Nishio-Hamane D, Ohnishi M, Momma K, Shimobayashi N, Miyawaki R, Minakawa T, Inaba S (2015) Imayoshiite, $Ca_3Al(CO_3)[B(OH)_4](OH)_6 \cdot 12H_2O$, a new mineral of the ettringite group from Ise City, Mie Prefecture, Japan. Mineral Mag 79:413–423

Peacor DR, Dunn PJ, Duggan M (1983) Sturmanite, a ferric iron, boron analogue of ettringite. Can Mineral 21:705–709

Pekov IV, Chukanov NV, Britvin SN, Kabalov YuK, Göttlicher J, Yapaskurt VO, Zadov AE, Krivovichev SV, Schüller W, Ternes B (2012) The sulfite anion in ettringite-group minerals: a new mineral species hielscherite, $Ca_3Si(OH)_6(SO_4)(SO_3) \cdot 11H_2O$, and the thaumasite–hielscherite solid-solution series. Mineral Mag 76:1133–1152

Pöllmann H, Kuzel H-J, Wenda R (1989) Compounds with ettringite structure. N Jb Min Abh 160:133–158

Pushcharovsky DY, Lebedeva YS, Zubkova NV, Pasero M, Bellezza M, Merlino S, Chukanov NV (2004) Crystal structure of sturmanite. Can Mineral 42:723–729

Ravel B, Newville M (2005) Athena, Artemis, Hephaestus: data analysis for X-ray absorption spectroscopy using IFEFFIT. J Synchrotron Radiat 12:537–541

Sheldrick GM (2008) A short history of *SHELX*. Acta Cryst A64:112–122

Sims I, Huntley SA (2004) The thaumasite form of sulfate attack—breaking the rules. Cement Concr Compos 26:837–844

Skoblinskaya NN, Krasilnikov KG, Nikitina LV, Varlamov VP (1975) Changes in crystal structure of ettringite on dehydration. 2. Cement Concr Res 5:419–431